Adaptive Regenerative Braking for Electric Vehicles with an Electric Motor at the Front Axle using the State Dependent Riccati Equation Control Technique

SVEN JANSEN, MOHSEN ALIREZAEI, STRATIS KANARACHOS
Technical Sciences
TNO
Steenovenweg 1, 5708 HN Helmond
THE NETHERLANDS
stratis.kanarachos@tno.nl http://www.tno.nl

Abstract: - In this paper a novel adaptive regenerative braking control concept for electric vehicles with an electric motor at the front axle is presented. It is well known that the "phased" type regenerative braking systems of category B maximize the amount of regenerative energy during braking. However, there is an increased risk of maneuvering capability loss especially during cornering. An integrated braking controller which determines - in a single step - the desired yaw moment and allocates the braking demand between hydraulic brakes and electric motor during cornering is designed using the State Dependent Riccati Equation (SDRE) method. A unique method for deriving the State Dependent Coefficient (SDC) formulation of the system dynamics is proposed. Soft constraints are included in the state dynamics while an augmented penalty approach is followed to handle hard constraints. The performance of the controller has been evaluated for different combined cornering-braking scenarios using simulations in a Matlab/Simulink environment. For this an eight degrees of freedom (DOF) nonlinear vehicle model has been utilized. The numerical results show that the controller is able to optimize (locally) the amount of regenerative braking energy while respecting system's constraints such as tire force saturation, vehicle yaw rate and slip angle errors.

Key-Words: - regenerative braking and cornering, stability, State Dependent Riccati Equation controller, optimization, state estimation

1 Introduction

In the automotive sector the rising fuel prices and the continuously stricter emissions legislation put pressure on the research and development of systems that can recuperate energy. Regenerative braking systems recover part of the kinetic energy by utilizing one or more electric motors during braking and therefore can substantially reduce fuel consumption and CO2 emissions. However, brake energy recovery is mainly limited by three factors: a) the maximum brake torque provided by the generator, b) the charge rate of the battery and c) the available tire-road friction. Due to above a braking system has to utilize also friction braking. Main subject of the present paper is the development of an integrated controller that maximizes the recuperated energy by optimally distributing the braking demand among the actuators while respecting system's constraints. The integrated controller has a coordination role and thus acts at a higher level. The lower level control part is not addressed in this paper.

Until now a number of studies have been conducted regarding different regenerative braking strategies and their implications on vehicle stability. For example, in reference Hancock et al [2012] a study regarding regenerative braking and its impact on vehicle's fuel economy and stability was presented. A regenerative braking system at the rear axle of a sport vehicle equipped with a conventional Anti-Lock Braking System and Electronic Stability Program was considered. The braking strategy was focused on maximizing the rear braking force. It was shown through simulations that in the case of low friction surfaces regenerative braking can significantly compromise vehicle stability during cornering. A solution proposed by the authors was to redistribute the regenerative braking force based on the actual wheel slip. The authors used a six body DOFs and four wheel rotational DOFs vehicle model. The tires were modeled according to the nonlinear Magic Formula Tire Model. Steering, driveline and suspension systems were assumed to be rigid bodies. Longitudinal and lateral weight transfer was considered.

Falcone et al [2009] studied the same problem but proposed a different solution. They have focused on cornering maneuvers on low friction surfaces, where excessive braking at the rear axle might induce vehicle instability. They have developed two model predictive controllers (MPC) based on different vehicle models and compared their performance. The objective was to maximize regenerative braking and distribute friction braking at the four wheels, while (a) delivering the braking force requested by the driver, (b) preserving vehicle stability and (c) fulfilling system constraints, e.g., bounds on regenerative braking set by the hybrid powertrain. The controllers were evaluated in a simulation environment for combined braking and cornering maneuvers.

Han et al [2011] studied the influence of regenerative braking on the dynamics of electric vehicles in case the electric motor is installed on the front axle. It was highlighted that excessive regenerative braking force distribution to the front axle can cause the vehicle to approach its handling limit earlier e.g. if the front tires saturate first, the vehicle may plow out of the curve. The solution proposed was an adaptive regenerative braking controller engaged when the vehicle comes in a danger of crossing the limit. The proposed controller has a two level structure. On the first level the desired direct yaw moment is calculated based on the LQR method and using the yaw rate and side slip angle errors. On the second level a numerical optimization algorithm splits the braking torque demand in a regenerative braking part for recovering the optimal braking energy and additional mechanical braking part for guaranteeing the lateral vehicle stability. The controller was tested in simulation for a severe cornering case.

Ólafsdóttir et al [2012] proposed for the same problem a nonlinear model predictive controller. The Model Predictive Control (MPC)-based approach solved the problem of blending friction and regenerative braking in order to satisfy the driver's braking request, while preserving the vehicle stability and drivability. The signals used by the proposed MPC controller were provided by a Vehicle State Estimator, which among others estimated also the road friction which is essential for the considered physical constraints. A two track vehicle model with three DOFs has been utilized. Normal load transfer due to lateral acceleration has been taken into account but neglecting the roll dynamics. The performance of the controller has been evaluated in a simulation environment.

The present study also considers a front-wheel-driven electric vehicle with an electric motor connected to the front drive axle. The friction braking system consists of an Electro-Mechanical-Brake system on the front wheels and an Electro-Hydraulic Brake system on the rear. The proposed controller computes doesn't separate the control problem in two stages a) first computed desired yaw moment and b) perform the control allocation. Instead it computes in one single step the braking command on each actuator in such a way that all control objectives are met. The controller is designed – to our knowledge for the first time- using the State Dependent Riccati Equation (SDRE) method. SDRE is a control technique which is rapidly emerging as general design and synthesis method of nonlinear feedback controllers for a broad class of nonlinear regulator problems. The performance of the controller is optimized with respect to an objective function which maximizes the regenerative braking energy in normal driving scenarios and keeps the vehicle stable in critical situations. SDRE has in general a significantly lower computational burden than Model Predictive Control (depending on the control horizon).

For the development of the controller the system equations are written in a State Dependent Coefficient (SDC) form based on the combined slip Magic Formula (MF) tire model and under the assumption that part of the vehicle states are estimated, e.g. Zuurbier et al [2002]. A novel numerical technique is proposed for deriving the SDC form. The SDRE controller computes the control inputs by solving a suboptimal control problem which seeks to minimize an objective function expressed as the the weighted sum of the overall control objectives. Tuning of the weights has been carried out by simulating different braking scenarios. Soft constraints such as tire saturation were included in the description of the system dynamics while an augmented penalty approach was used for the hard constraints. Due to the state dependency of the system matrices less tuning effort is required compared to gain scheduling methods. The performance of the controller has been evaluated for different scenarios using simulations in a Matlab/Simulink environment. A nonlinear eight degrees of freedom (DOFs) vehicle model has been utilized. The results show that the integrated controller performs well in maximizing the regenerative braking effort in normal driving scenarios and in keeping the vehicle stable and maneuverable under extreme cornering.

The rest of the paper is organized as follows. In Section 2 the mathematical model used is presented, while in Section 3 the design of the regenerative braking controller is discussed in detail. In Section 4

the performance of the controller is evaluated for different case studies. In Section 5 conclusions and future research directions are drawn.

2 Mathematical Model

2.1 Vehicle model

The vehicle model used for the development of the SDRE controller is shown in Figure 1. According to Pacejka ([2005] [6]) it is a model that is suitable for nonlinear non steady handling maneuvers studies.

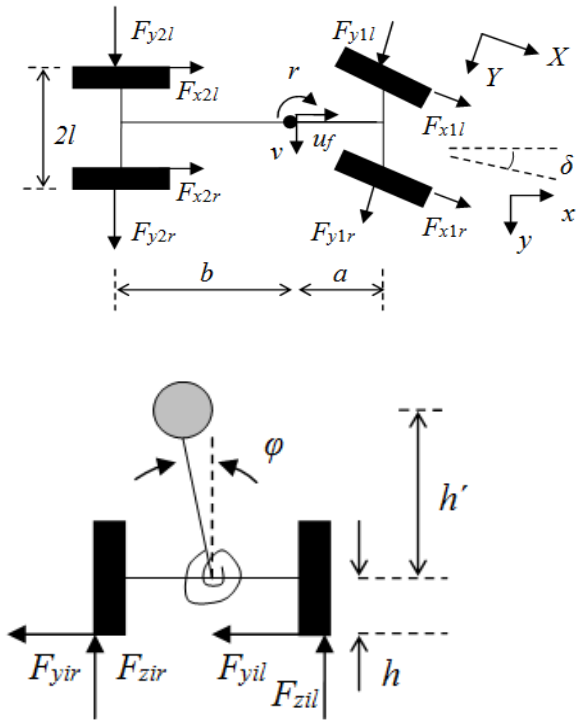

Figure 1. Top (upper) and front (lower) view of the vehicle model

The architecture of the braking system is shown in Figure 2. The front friction brakes are actuated by an electro-mechanical brake system while the rear from an electro-hydraulic one. At the front axle an electric motor with regenerative capability is installed. In this study the effect of the different actuator's dynamics on the transient braking performance isn't considered in detail. To be more precise, the dynamics of the actuators is neglected and the braking input is processed by a first order filter that matches the slowest actuator dynamics.

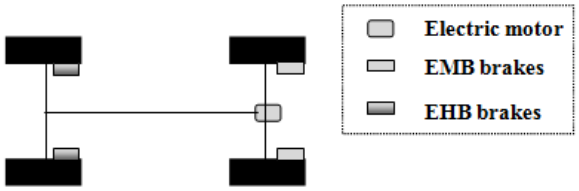

Figure 2. Architecture of braking system

The vehicle model has eight degrees of freedom that describe the vehicle's forward u_f, lateral v, yaw r, roll φ and the four wheel angular ω_1, ω_2, ω_3 and ω_4 motions. Shock absorbers in the wheel suspensions are represented by damping coefficients $k_{\varphi i}$ at the front and rear axles, i=1, 2 respectively. In an analogous manner the suspension springs $c_{\varphi i}$ are modelled. The roll angle, the steer angle and the roll axis inclination are considered small enough for linearization purposes. The effects of additional steer angles due to suspension kinematics and steer compliance are neglected. Coriolis forces which act in the longitudinal direction are negligible and therefore aren't considered (see e.g. Ryu [2004]).

$$m\cdot\left(\dot{u}_f - r\cdot v - h'\cdot\varphi\cdot\dot{r} - 2\cdot h'\cdot r\cdot\dot{\varphi}\right) = F_{x1r} + F_{x1l} + F_{x2r} + F_{x2l} \tag{1}$$

$$m\cdot\left(\dot{v} + r\cdot u_f + h'\cdot\ddot{\varphi} - h'\cdot r^2\cdot\varphi\right) = F_{y1r} + F_{y1l} + F_{y2r} + F_{y2l} \tag{2}$$

$$I_z\cdot\dot{r} + (I_z\cdot\theta_r - I_{xz})\cdot\ddot{\varphi} - m\cdot h'\cdot\left(\dot{u}_f - r\cdot v\right)\cdot\varphi = a\cdot F_{y1r} + a\cdot F_{y1l} - b\cdot F_{y2r} - b\cdot F_{y2l} \tag{3}$$

$$\left(I_x + mh'^2\right)\cdot\ddot{\varphi} + m\cdot h'\cdot\left(\dot{v} + r\cdot u_f\right) + (I_z\cdot\theta_r - I_{xz})\cdot\dot{r} - \left(m\cdot h'^2 + I_y - I_z\right)\cdot r^2\cdot\varphi + \left(k_{\varphi 1} + k_{\varphi 2}\right)\cdot\dot{\varphi} + \left(c_{\varphi 1} + c_{\varphi 2} - m\cdot g\cdot h'\right)\cdot\varphi = 0 \tag{4}$$

$$I_w\cdot\dot{\omega}_{1r} = M_{br1r} - F_{x1r}\cdot R \tag{5}$$

$$I_w\cdot\dot{\omega}_{1l} = M_{br1l} - F_{x1l}\cdot R \tag{6}$$

$$I_w\cdot\dot{\omega}_{2r} = M_{br2r} - F_{x2r}\cdot R \tag{7}$$

$$I_w\cdot\dot{\omega}_{2l} = M_{br2l} - F_{x2l}\cdot R \tag{8}$$

where m is the vehicle's mass, I_x the roll moment of inertia, I_z the yaw moment of inertia, I_y the pitch moment of inertia, I_{xz} the respective product

moment of inertia. Subscripts *r* and *l* denote right and left wheel respectively. I_w is the effective wheel's moment of inertia, *R* is the wheel radius and the braking moments M_{br} are expressed as:

$$M_{br1r} = M_{fr1r} + M_{rb}/2 \quad (9)$$

$$M_{br1l} = M_{fr1l} + M_{rb}/2 \quad (10)$$

$$M_{br2r} = M_{fr2r} \quad (11)$$

$$M_{br2l} = M_{fr2l} \quad (12)$$

With M_{fri} is denoted the braking moment induced by the friction brakes at a wheel on the i^{th} axle and with M_{rb} the regenerative braking moment induced by the electric motor on the front axle. An equal split of the regenerative braking moment to the left and right front wheel has been assumed. The vehicle's parameters used in this study are listed in Table 1.

Name	Parameter	Value
Vehicle mass	m [kg]	1737
Distance from roll axis to CG	h' [m]	0.51
Distance of front axle from CG	a [m]	1.4591
Distance of rear axle from CG	b [m]	1.2429
Roll axis angle with XY plane	θ_r [rad]	0.043
Moment of inertia - to *z* axis	I_z [kgm^2]	2877
Moment of inertia - *y* axis	I_y [kgm^2]	1500
Moment of inertia - *x* axis	I_x [kgm^2]	500
Roll damping axle *i*	$k_{\varphi i}$ [Ns/rad]	800
Roll stiffness axle *i*	$c_{\varphi i}$ [N/rad]	30000
Half length of the wheel axle	l [m]	0.765
Height from ground to roll axis at C.oG.	h [m]	0.0707
Wheel moment of inertia	I_w [kgm^2]	1.1

The vertical loads F_{zir} and F_{zil} on the tires are not constant during the manoeuvre. The vertical load transfer is obtained by considering the moment equilibrium of the front and rear axle about the respective roll centres. Thus the roll moments resulting from suspension springs and dampers and the axle side forces are regarded. More specific we have:

$$F_{z1r} = 0.5\frac{m \cdot g \cdot b}{a+b} + \Delta F_{zi} \quad (13)$$

$$F_{z1l} = 0.5\frac{m \cdot g \cdot b}{a+b} - \Delta F_{zi} \quad (14)$$

$$F_{z2r} = 0.5\frac{m \cdot g \cdot a}{a+b} + \Delta F_{zi} \quad (15)$$

$$F_{z2l} = 0.5\frac{m \cdot g \cdot a}{a+b} - \Delta F_{zi} \quad (16)$$

where the vertical load transfer is:

$$\Delta F_{zi} = \frac{-c_{\varphi i} \cdot \varphi - k_{\varphi i} \cdot \dot{\varphi} + \left(F_{yri} + F_{yli}\right) \cdot h}{2 \cdot l} \quad (17)$$

2.2 Tire model

The tire model used for the expressing the tire force is a combined slip Magic Formula tire model. In case of pure side slip the lateral tire force F_{y0} is described by:

$$F_{y0}(\alpha_S) = D \cdot \sin\left(C \cdot \arctan\left(\begin{matrix} B \cdot \alpha_S - E \cdot \\ \left(B \cdot \alpha_S - \arctan\left(B \cdot \alpha_S\right)\right) \end{matrix}\right)\right) \quad (18)$$

where $\alpha_S = \tan(\alpha)$ is the slip angle, $D = \mu \cdot F_z$ the peak value, C the shape factor, E the curvature factor $B = C_{F\alpha} / C \cdot D$ the stiffness factor and μ the tire-road friction coefficient. The tires' parameters are shown in Table 2.

Table 2 Tire parameters.

Name	Parameter	Value
Shape factor	C	1.3
Tire-road friction coefficient	μ	0.1-0.8
Curvature factor	E	-3

Coefficient	$C_{F\alpha} = c_1 \cdot \sin\left(2 \cdot \arctan\left(\frac{F_z}{c_2}\right)\right)$	
Maximum cornering stiffness [N/rad]	c_1	60000
Load at max. cornering stiffness [N]	c_2	4000

The slip angles α_1 and α_2 of the forward and rear wheels are considered small ($\sin\alpha_i \approx \alpha_i$) and are computed according to:

$$\alpha_1 = \delta - \frac{1}{u_f} \cdot (v + a \cdot r) \qquad (19)$$

$$\alpha_2 = -\frac{1}{u_f} \cdot (v - b \cdot r) \qquad (20)$$

where δ is the steer angle. For the purpose of this study, we have assumed that the slip angles for both left and right wheels are equal ($\alpha_{1r} = \alpha_{1l} = \alpha_1$ and $\alpha_{2r} = \alpha_{2l} = \alpha_2$). This is a valid assumption when $l \cdot |r| << u_f$ (Pacejka [2005]).

In an analogous manner in case of pure longitudinal slip longitudinal force F_{x0} is expressed as:

$$F_{x0} = D_x \cdot \sin\left(C_x \cdot \arctan\left(B_x \cdot \kappa - E_x \cdot \left(B_x \cdot \kappa - \arctan(B_x \cdot \kappa)\right)\right)\right) \qquad (21)$$

where κ is the longitudinal slip.

In case of combined slip longitudinal and lateral forces are expressed as a function of the pure longitudinal F_{x0} and lateral forces F_{y0} multiplied by the weighting functions G_{xa} and G_{yk}:

$$F_x = G_{xa} \cdot F_{x0} \qquad (22)$$

$$F_y = G_{yk} \cdot F_{y0} \qquad (23)$$

where C_x is the average longitudinal tire stiffness and C_y the average lateral tire stiffness.

A graphical illustration of the weighting function $G_{yk} = F_y / F_{y0}$ for a particular tire model (205/60R15) included in the MF-Tire database is shown in Figure 3.

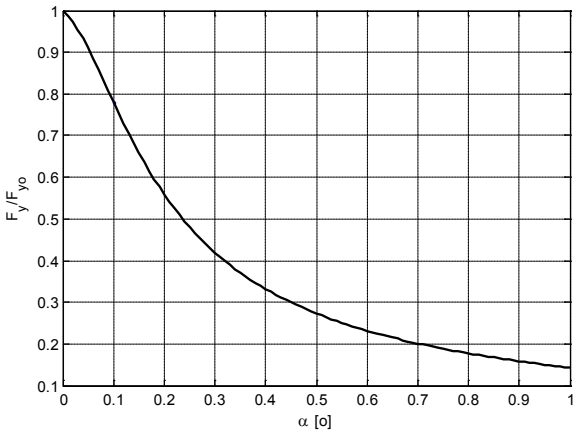

Figure 3. Normalized lateral force reduction F_y/F_{y0} versus longitudinal slip κ for a slip angle a =5°.

2.3 Motor model

The electric motor is modelled as a look-up table with motor-generator characteristics of a permanent magnet synchronous machine from the ADVISOR database (Markel et al (2002)). The motor model uses lookup tables for defining torque and efficiency characteristics of the motor. A two column lookup table is used to determine the maximum torque that the motor can generate. The first column holds the speeds of the motor while the second holds the maximum drive torque that the motor can generate for the corresponding speed.

Figure 4 shows the efficiency map of the motor at various operating points. The efficiency of the motor is determined using a 3D lookup table. The first two dimensions of the lookup table form the motor speed vs. torque grid and the last dimension holds the efficiency values for the corresponding operating points. Note that brake torque for recuperation reduces to zero for low motor speeds (indicated by shaded area).

2.4 Battery model

The battery model, similar to the motor, uses lookup tables to define changing resistance Rl and voltage levels U_{oc} as function of the State of Charge (SoC). The battery has the battery characteristics of a Lithium-Ion battery from ADVISOR 3.0. The battery's open circuit voltage, charging resistance

and discharging resistance are all determined by the use of two column lookup tables (Varocky [2011]).

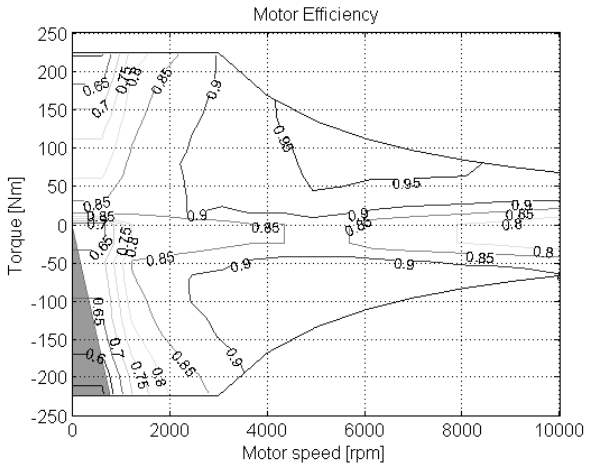

Figure 4. Motor efficiency map for MC_PM49 electric motor.

3 The SDRE Controller

A signal flow diagram of the braking control system is shown in Figure 5. With EHB we denote the Electro-Hydraulic Brakes, EMB the Electro-Mechanical Brakes and VSE the Vehicle State Estimator. The Vehicle State Estimator – an implementation of the Extended Kalman Filter concept (Leenen et al [2010]) - filters the noisy sensor signals and estimates non-measurable variables like the vehicle slip angle. The battery module feeds the supervisor module regarding recharging capability. The supervisor module generates the reference commands, sets the system's constraints and communicates system faults. The SDRE module performs the control allocation task. The dedicated local controllers –not covered in this study- track the desired set points by controlling the brakes and the electric motor.

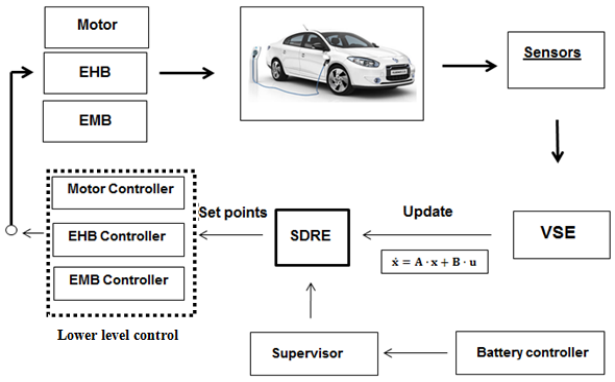

Figure 5. Components and signal flow of the control system.

The SDRE control module shown in Figure 6 performs four functions: a) formulates the system dynamics in the SDC form b) computes the objective function value based on the overall objectives c) calculates the feedback gain and d) computes the set points.

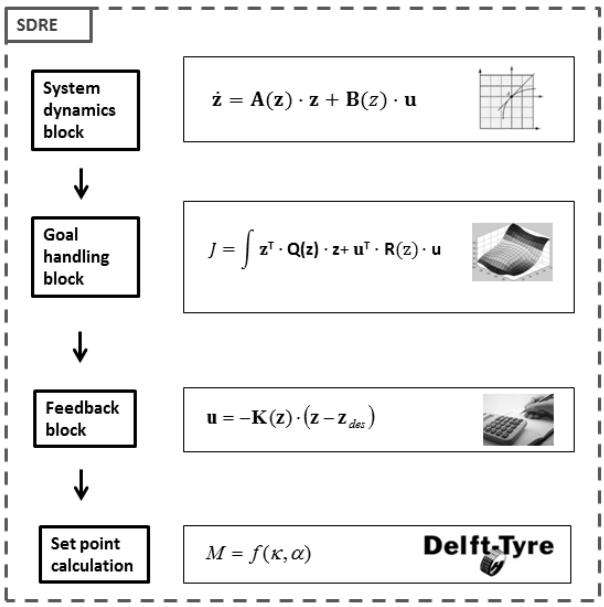

Figure 6. Main blocks of SDRE control module.

3.1 The system dynamics block

In SDRE the nonlinear dynamics of the system is factorized into the state vector and the product of a matrix valued function that depends on the state itself. In doing so, the nonlinearities of the system are fully captured bringing the nonlinear system to a linear like structure having state-dependent coefficient (SDC) matrices, see Cloutier et al.

The first step in deriving the SDC form is to express the vehicle's equations of motion (1-8) as a system of first order differential equations. With the model set up used there are nine differential equations of first order and consequently five state variables $\mathbf{z} = \begin{bmatrix} u_f & v & r & \varphi & \dot{\varphi} \end{bmatrix}^T$. In order to apply the SDRE control technique, the system's equations (24) have to be written in a linear like state space form:

$$\dot{\mathbf{z}}(t) = \mathbf{A}(\mathbf{z}) \cdot \mathbf{z} + \mathbf{g} \cdot \mathbf{u} \qquad (24)$$

In Appendix 1 a description of (28) is given.

Equation (29) is the so called SDC formulation of the system because matrix $\mathbf{A}(\mathbf{z})$ is dependent on

the state $\mathbf{z}$. A difficulty in transforming Equations (1)-(8) into the SDC form is the combined slip tire behavior. To circumvent this, most of the researchers implement a decoupled tire model (Bonsen et al [2010]) which doesn't consider the interaction between lateral and longitudinal slip force characteristics. However, the influence of longitudinal slip on the lateral force at high slips is significant (see Figure 3). The following formulation has been proposed (Alirezaei et al [2013]) to express the combined slip tire behaviour:

$$F_x(\kappa,\alpha) = G_{x\alpha}(\kappa,\alpha)\cdot F_{x0} = C_{x1}(\kappa,\alpha)\cdot\kappa + C_{x2}(\kappa,\alpha)\cdot\alpha \quad (25)$$

$$F_y(\kappa,\alpha) = G_{yk}(\kappa,\alpha)\cdot F_{y0} = C_{y1}(\kappa,\alpha)\cdot\kappa + C_{y2}(\kappa,\alpha)\cdot\alpha \quad (26)$$

Generally, there are infinite ways to determine the coefficients $C_{x1}(\kappa,\alpha)$, $C_{x2}(\kappa,\alpha)$, $C_{y1}(\kappa,\alpha)$ and $C_{y2}(\kappa,\alpha)$ (see e.g. Cimen [2008]). In this study a numerical procedure is proposed. The calculation of C_{x1}, C_{x2}, for a pair $\mathbf{s} = [\kappa \quad \alpha]^T$ is performed as follows:

$$C_{x1} = \frac{\delta F_x(\delta\kappa,0)}{\delta\kappa} = \frac{F_x(\kappa,0)}{\kappa} \quad (27)$$

and by substituting (27) in (25) we get:

$$C_{x2} = \frac{G_{x\alpha}(\kappa,\alpha)\cdot F_{x0} - C_{x1}\cdot\kappa}{\alpha} \quad (28)$$

In an analogous manner C_{y1} and C_{y2} are computed:

$$C_{y2} = \frac{\delta F_y(0,\delta a)}{\delta a} = \frac{F_y(0,a)}{\alpha} \quad (29)$$

and by substituting (29) in (26) we get:

$$C_{y1} = \frac{G_{y\kappa}(\kappa,\alpha)\cdot F_{x0} - C_{y2}\cdot\alpha}{\kappa} \quad (30)$$

3.2 Feedback gain calculation

The feedback gain calculation for the SDRE controller is based on the LQR theory. At each sampling instant the state dependent coefficient matrix $\mathbf{A}(\mathbf{z})$ is considered to be frozen and the feedback $\mathbf{u}$ of an optimal LQR regulator is computed.

$$\mathbf{u} = -\mathbf{K}\cdot(\mathbf{z} - \mathbf{z}_{des}) \quad (31)$$

where $\mathbf{z}_{des}$ is the desired state vector and $\mathbf{K}$ the feedback gain.

The feedback gain $\mathbf{K}$ of the SDRE controller is computed by minimizing a quadratic like objective function expressed as:

$$J = \int_0^\infty \left(\mathbf{z}^T\cdot\mathbf{Q}\cdot\mathbf{z} + \mathbf{u}^T\cdot\mathbf{R}\cdot\mathbf{u}\right)\cdot dt \quad (32)$$

where $\mathbf{Q} = diag(1,0.01,0.01,0.001)$ and $\mathbf{R} = diag(1,1,1,1,0.05)$. The reason for choosing $\mathbf{R}(5,5) = 0.05$ and $\mathbf{R}(1,1) = \mathbf{R}(2,2) = \mathbf{R}(3,3) = \mathbf{R}(4,4) = 1$ is to maximize the amount of recuperative energy.

The state feedback gain $\mathbf{K}(\mathbf{z})$ is computed according to

$$\mathbf{K} = \mathbf{R}(\mathbf{z})^{-1}\cdot\mathbf{B}(\mathbf{z})^T\cdot\mathbf{P}(\mathbf{z}) \quad (33)$$

where $\mathbf{P}(\mathbf{z})$ is the solution of the Algebraic State Dependent Riccati Equation,

$$\mathbf{A}(z)^T\cdot\mathbf{P}(z) + \mathbf{P}(z)\cdot\mathbf{A}(z) - \mathbf{P}(z)\cdot\mathbf{B}\cdot\mathbf{R}(z)^{-1}\cdot\mathbf{B}(z)^T\cdot\mathbf{P}(z) + \mathbf{Q}(z) = 0 \quad (34)$$

Several numerical methods have been developed for solving the algebraic Riccati equation. In this study a modification of the Kleinman algorithm with a maximum number of iterations has been applied. The controller has been applied real time on a prototype vehicle (Alirezaei et al [2013]).

3.3 Constraints and goal handling

In the present study the maximum amount of regenerative braking is dependent on the available tire road friction coefficient at the front wheels and the speed dependent maximum torque delivered by the electric motor.

In order to account for the system's constraints the original objective function to be minimized, Equation (32), is augmented by two additional terms shown in Equation (35):

$$J = \int_0^\infty \left(\begin{array}{c} \mathbf{z}^T\cdot\mathbf{Q}\cdot\mathbf{z} + \mathbf{z}^T\cdot\mathbf{W}_z(\mathbf{z})\cdot\mathbf{z} + \\ \mathbf{u}^T\cdot\mathbf{R}\cdot\mathbf{u} + \mathbf{u}^T\cdot\mathbf{W}_u(\mathbf{u})\cdot\mathbf{u} \end{array} \right)\cdot dt \quad (35)$$

The coefficients in matrices $\mathbf{W}_z(\mathbf{z}) = diag(w_{z1}, w_{z2}, ..., w_{z5})$ and $\mathbf{W}_u(\mathbf{u}) = diag(w_{u1}, w_{u2}, ..., w_{u5})$ are :

$$w_{zi}(\mathbf{z}) = \frac{1}{\left(\left\|h_i(\mathbf{z})\right\|\right)^2 + \sigma_{zi}^2} \quad (36)$$

$$w_{ui}(\mathbf{u}) = \frac{1}{\left(\left\|g_i(\mathbf{u})\right\|\right)^2 + \sigma_{ui}^2} \quad (37)$$

where $\left\|h_i(\mathbf{z})\right\|$ is the distance between the state vector $\mathbf{z}$ and its boundary, $\left\|g_i(\mathbf{u})\right\|$ is the distance between the control vector $\mathbf{u}$ and its boundary and σ_{zi}, σ_{ui} user defined constants.

4 Numerical Evaluation

The performance of the proposed controller has been evaluated using simulations for an extensive number of driving scenarios. The simulations are performed in a Matlab/Simulink environment and are based on the vehicle data shown in Table 1 and the tire parameters shown in Table 2. The vehicle data are representative of a prototype electric vehicle.

For brevity only three test cases will be discussed in the following subsections. These illustrate the braking performance during cornering at a low μ surface for three different braking intensities. The results are discussed and the merit of implementing a nonlinear control allocator which considers tire nonlinearities is highlighted.

4.1 Braking scenario 1: Braking and cornering on a low μ=0.3 surface. Desired deceleration 0.58 m/s^2

The vehicle is moving with 100 *km/h* on a low friction μ=*0.3* surface. At time *t*=3 *s* the driver commands a steering input which is illustrated in Figure 7 (upper part). The vehicle starts cornering and after a transient period it reaches a steady state response. At time *t*=14 *s* the driver induces a braking command as shown in Figure 7 (lower part). For comparison reasons the numerical results for two different tunings parameter sets will be shown. In the first case the SDRE control law is applied with $\mathbf{Q}_1 = diag(1,0,0,0)$. With this tuning set lateral velocity *v* and yaw rater *r* errors are neglected. In the second case $\mathbf{Q}_2 = diag(1,0.01,0.01,0.001)$. The numerical results for the two cases are shown in the following figures (upper part: $\mathbf{Q}_1$, lower part: $\mathbf{Q}_2$). In Figure 8 the path followed by the vehicle is shown while in Figure 9 the distance error (deviation). At time *t*=20 *s* the deviation in the first case is 1.5 *m* while in the second 1.1 *m*. Regarding recuperated energy in the first case 69777 *J* were recuperated with a 63% efficiency while in the second case 70000 *J* with a 63.2% efficiency. Both cases have almost the same recuperation efficiency however the tracking performance is better in the second one.

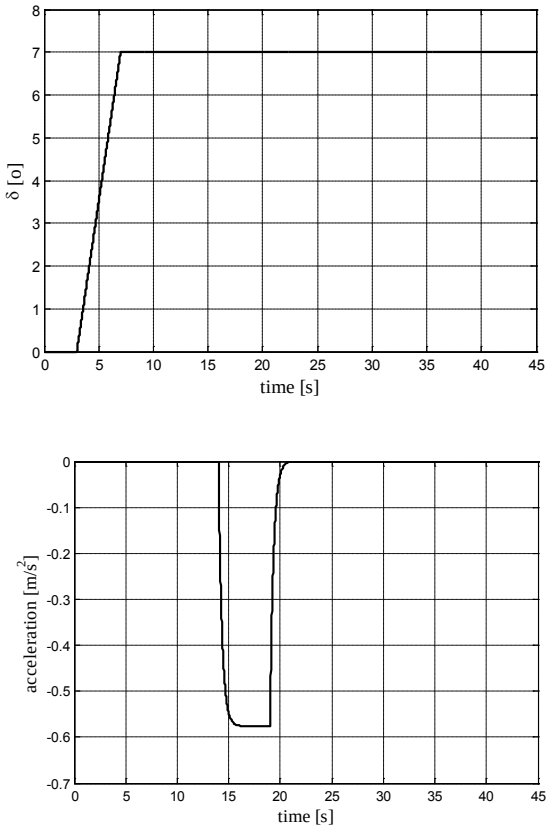

Figure 7. Steering (upper) and braking (lower) command induced by driver for the first scenario

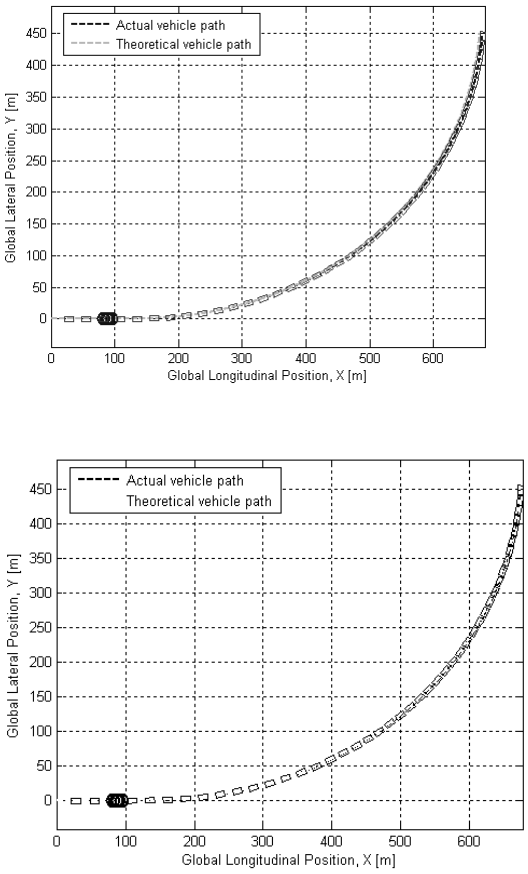

Figure 8. Vehicle trajectory (upper part: $\mathbf{Q}_1$ case, lower part: $\mathbf{Q}_2$ case) in the first scenario.

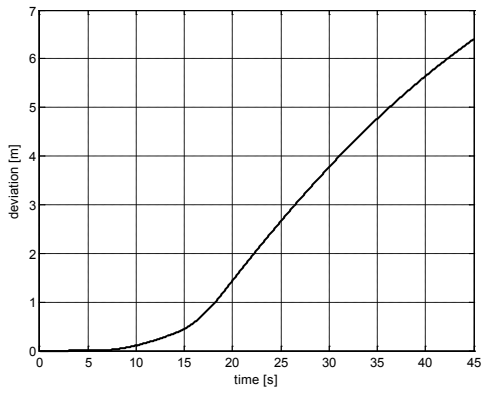

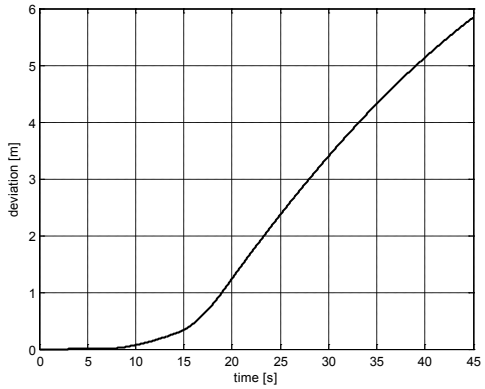

Figure 9. Deviation in *m* from nominal path (upper part: $\mathbf{Q}_1$ case, lower part: $\mathbf{Q}_2$ case) in the first scenario.

4.2 Braking scenario 2: Braking and cornering on a low μ=0.3 surface. Desired deceleration 1.18 m/s^2

The vehicle is moving with 100 *km/h* on a low friction $\mu=0.3$ surface. At time t=3 *s* the driver induces a steering command shown in Figure 10 (upper part). At time t=14 *s* the driver induces a braking command as shown in Figure 10 (lower part). Again the numerical results for the two cases will be shown (upper– lower part respectively). In Figure 11 the path followed by the vehicle is shown while in Figure 12 the distance error (deviation). At time t=20 *s* the deviation in the first case is 3.8 m while in the second 1.8 *m*. Regarding the recuperated energy in the first case $1.22 \cdot 10^5$ *J* were recuperated with a 61% efficiency while with the second configuration $4.8 \cdot 10^4$ *J* with a 23.35% efficiency. It is evident that in the first case a significantly higher amount of energy is recuperated (almost 2.6 times better efficiency) however the tracking performance is worse (2.11 times worse). In Figure 13 the total force on each wheel as well as their maximum values are shown. As may be observed the braking induced at the front wheels causes the tire forces to enter the nonlinear region (Figure 13 – upper part) and results in bad tracking performance. Instead in the second case the controller "senses" that the tires enter the nonlinear region and redistributes accordingly the braking command between the front and rear tires.

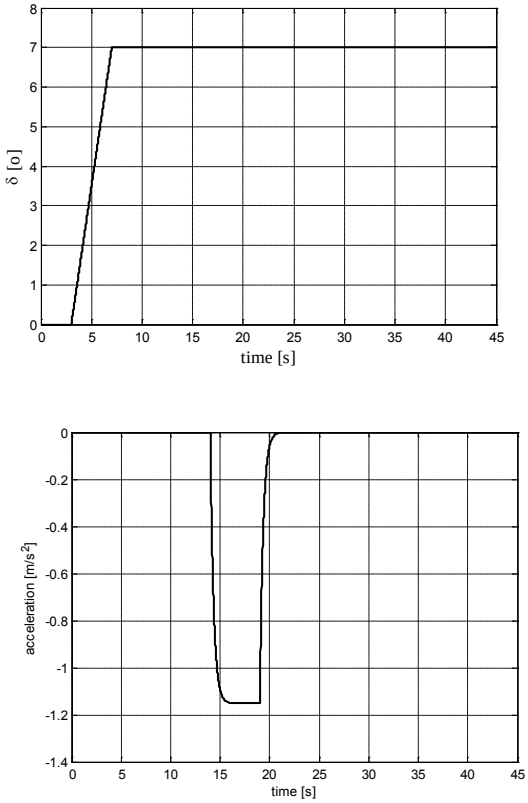

Figure 10. Steering and braking command induced by driver in the second scenario.

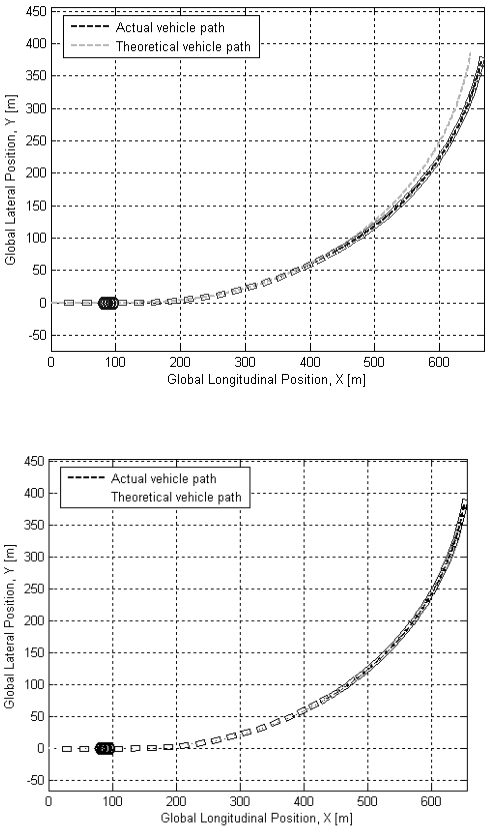

Figure 11. Vehicle trajectory (upper part: $\mathbf{Q}_1$ case, lower part: $\mathbf{Q}_2$ case) for the second scenario.

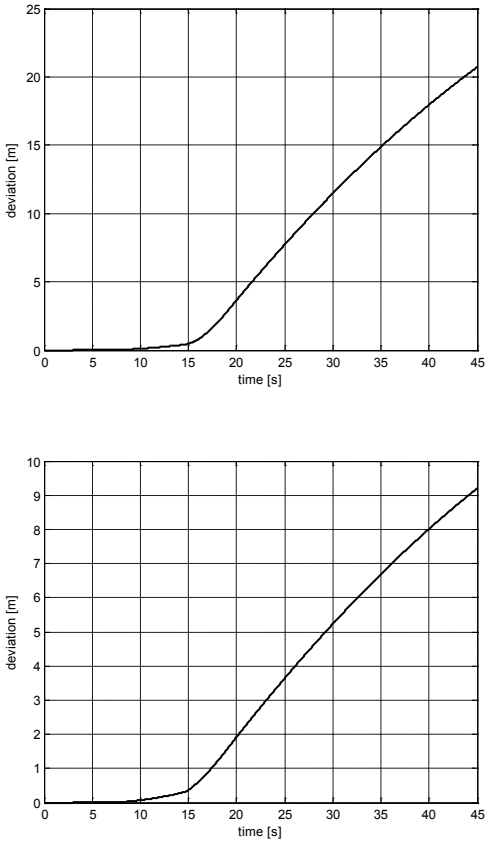

Figure 12. Deviation in m from desired path (upper part: $\mathbf{Q}_1$ case, lower part: $\mathbf{Q}_2$ case) in the second scenario.

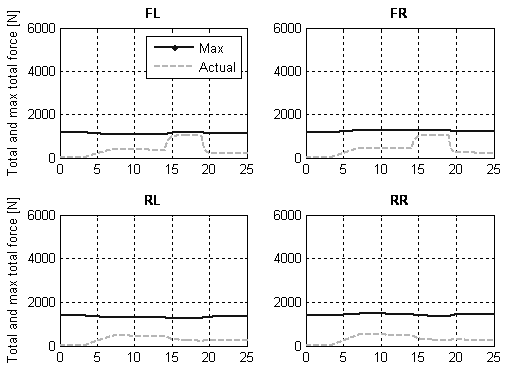

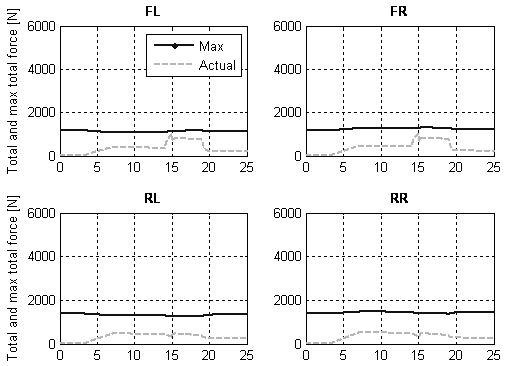

Figure 13. Total force per wheel and their maximum values (upper part: $\mathbf{Q}_1$ case, lower part: $\mathbf{Q}_2$ case) in the second scenario (FL: front left, FR: front right, RL: rear left, RR: rear right).

4.3 Braking scenario 3: Braking and cornering on a low μ=0.3 surface. Desired deceleration 1.72 m/s^2

The vehicle is moving with 100 km/h on a low friction $\mu=0.3$ surface. At time t=3 s the driver induces a steering command shown in Figure 7 (upper). At time t=14 s the driver induces a braking command which corresponds to a deceleration of 1.72 m/s^2. The numerical results for the two cases will be shown as previously in two part figures (upper – lower respectively). In Figure 14 the deviation for both cases is shown. In the first case at t=20 s a deviation of almost 10.2 m from the nominal path can be observed. Contrary in the second a deviation of only 2.8 m. The recuperated energy in the first case is 4.0 $\cdot 10^4$ J and the regenerative efficiency 14.2%. In the second case the recuperated energy is 4.7 $\cdot 10^4$ J and the achieved efficiency 16.8%. The braking force distribution for both cases is shown in Figure 15. It is obvious that in the first case the front tire forces saturate due to the application of regenerative braking. In the second case the vehicle presents better tracking performance compared to the first case but with the same regenerative braking efficiency.

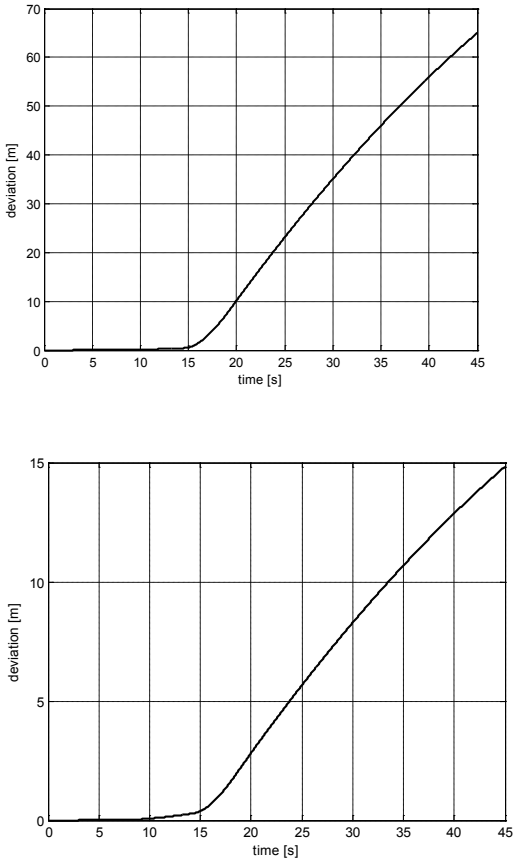

Figure 14. Deviation in m from desired path (upper part: $\mathbf{Q}_1$ case, lower part: $\mathbf{Q}_2$ case in the third scenario.

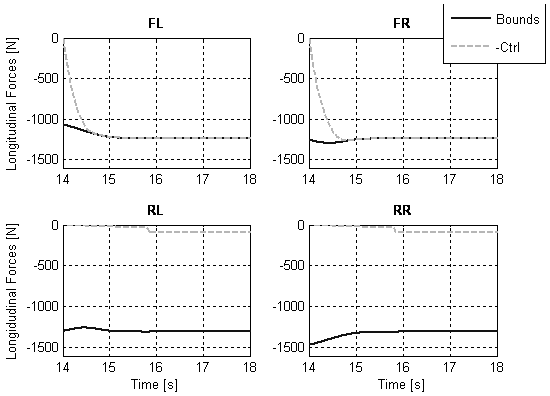

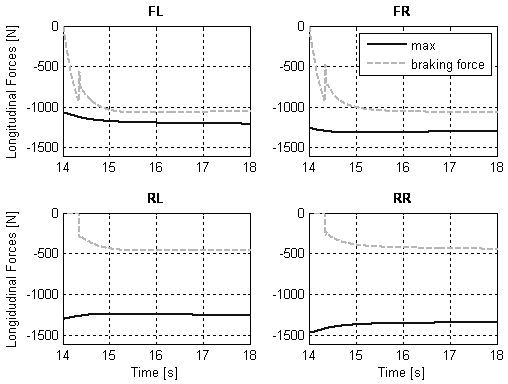

Figure 15. Braking force distribution (upper part: $\mathbf{Q}_1$ case, lower part: $\mathbf{Q}_2$ case) in the third scenario.

5 Conclusion

In this study the development of an integrated braking controller that maximizes (in the vicinity of the operating point) regenerative braking power for an electric vehicle with a motor at its front axle has been presented. The focus of the study was to design –using a standardized method- a nonlinear braking control law which determines - in a single step - the desired yaw moment and allocates the braking demand between hydraulic brakes and electric motor during cornering. As a result the controller achieves to optimize a) the amount of energy recuperated and b) the tracking performance of the vehicle.

A novel method has been proposed for constructing numerically the State Dependent Coefficient (SDC) form of the vehicle system based on the output of a Vehicle State Estimator and the Magic Formula tire model. The feedback gain is calculated by minimizing an objective function which is the weighted square sum of the systems' state errors and control inputs. Soft constraints such as tire saturation are included in the state dynamics while hard constraints are being considered using an augmented penalty approach. An algebraic Riccati equation (ARE) is solved on-line to give the suboptimum control law.

The performance of the controller has been evaluated for different combined braking and cornering scenarios using simulations in a Matlab/Simulink environment. The numerical investigations have shown the ability of the proposed SDRE controller to brake the vehicle with a force distribution that maximizes regenerative braking (in the vicinity of the operating point) while respecting maximum values of yaw rate and slip angle error.

The proposed SDC form for the vehicle with the combined slip tire model provides the appropriate framework to include more actuators like active suspension and active steering in the control system. Including in the model the shaft torsional stiffness as well as the actuators' dynamics are future research subjects.

Acknowledgments

This work is part of the European Commission's co-funded research project ID4EV (Intelligent Dynamics for Fully Electric Vehicles) under the 7th Framework programme (FP 7) and the national HTAS-EVT programme.

References:

[1]Hancock, M. and Assadian, F. Impact of regenerative braking on vehicle stability. In: *Proceedings of IET Hybrid Vehicle Conference,* Coventry, UK, 12-13 December 2006, pp. 173-184.

[2]Falcone, P., Khoshfetrat Pakazad S. and S. Solyom, Predictive Approaches to Rear Axle Regenerative Braking Control in Hybrid Vehicles, In: *Proceedings of Joint 48th IEEE Conference on Decision and Control and 28th Chinese Control Conference* Shanghai, P.R. China, 16-18 December, 2009, pp. 7627-7632.

[3]Han, J., Park, Y. and Park, Y., Adaptive regenerative braking control in severe cornering for guaranteeing the vehicle stability of fuel cell hybrid electric vehicle, In: *Proceedings of the Vehicle Power and Propulsion Conference* , 6-9 Sept. 2011, pp. 1-5.

[4]Ólafsdóttir, JM., Lidberg, M., Falcone, P., Energy recuperation in fully electric vehicles subject to stability and drivability requirements, In: *Proceedings of the 11th Inernational Symposium on Advanced Vehicle Control*, 9-12 September 2012, Seoul, Korea, pp. 1-6.

[5]Zuurbier, J. and Bremmer, P. State Estimation for Integrated Vehicle Dynamics Control. In: *Proceedings of the 6th International Symposium on Advanced Vehicle Control,* Hiroshima, Japan, 9-14 Septmeber 2002, pp. 1-6.

[6]Pacejka, B. *Tire and Vehicle Dynamics*. Warrendale, Society of Automotive Engineers, 2005.

[7]Ryu, J. *State and parameter estimation for vehicle dynamics control using GP*S. Phd Thesis, Mechanical Engineering Department, Stanford, 2004.

[8]Markel, T., Brooker, A. , Hendricks, T., Johnson, V. , Kelly, K., Kramer, B., O'Keefe, M., Sprik, S. and Wipke, K. ADVISOR: a systems analysis tool for advanced vehicle modeling. *Journal of Power Sources* 2002; 110 (1): pp. 255–266.

[9]Varocky, B. *Benchmarking of regenerative braking for a fully electric car*, Report No. D&C 2011.002, MSc Thesis, Eindhoven University of Technology, 2011.

[10] Leenen, R. Schouten, H. Virtual Sensors for Advanced Vehicle Stability Control, In: *Proceedings of the 10th International Symposium on Advanced Vehicle Control*, Loughborough, UK, 22-27 August 2010, pp. 7-13.

[11] Cloutier, J.R., C.N. D'Souza and C.P. Mracek. Nonlinear regulation and nonlinear H∞ control via the state-dependent Riccati equation technique: Part 1, Theory; Part 2, Examples. In: *Proceedings of the First International Conference on Nonlinear Problems in Aviation and Aerospace*, 9-11 May 1996, Florida, USA, pp. 117-141.

[12] Bonsen, E. Mansvelders, E. Vermeer. Integrated Vehicle Dynamics Control using the State B. Dependent Ricatti Equation method, In: *Proceedings of the 10th International Symposium on Advanced Vehicle Control*, Loughborough, UK, 22-27 August 2010, pp. 1-6.

[13] Alirezaei, M.; Kanarachos, S.; Scheepers, B.; Maurice, J.P., Experimental evaluation of optimal Vehicle Dynamic Control based on the State Dependent Riccati Equation technique, *Proceedings of the American Control Conference (ACC), 2013* , vol., no., pp.408,412, 17-19 June 2013

[14] Cimen, T. State-Dependent Riccati equation (SDRE) control: A Survey. In: *Proceedings of the 17th World Congress The International Federation of Automatic Control*, Seoul, Korea, 6-11 July 2008, pp. 3761-3775.

Appendix 1

SDC form

The SDC form of the vehicle system is expressed as follows:

$$\begin{aligned}\dot{u}_f = &\left(\frac{h'\cdot\dot{r}\cdot m\cdot R^2}{m\cdot R^2+4\cdot I_w}\right)\cdot\varphi+\\ &\left(\frac{r\cdot m\cdot R^2}{m\cdot R^2+4\cdot I_w}\right)\cdot v+\\ &\left(\frac{2\cdot h'\cdot\dot{\varphi}\cdot m\cdot R^2}{m\cdot R^2+4\cdot I_w}\right)\cdot r+\\ &\frac{R}{m\cdot R^2+4\cdot I_w}\cdot\begin{bmatrix}M_{fr1r}\\M_{fr1l}\\M_{fr2r}\\M_{fr2l}\\M_{rb}\end{bmatrix}\end{aligned}$$

$$\begin{aligned}\dot{v} = &\left(-r\right)\cdot u_f+\left(h'\cdot r^2\right)\cdot\varphi-\\ &\frac{\left(C_{y1r}+C_{y1l}\right)-\left(C_{y2r}+C_{y2l}\right)}{m\cdot u_f}\cdot v-\\ &\frac{\left(C_{y1r}+C_{y1l}\right)\cdot a+\left(C_{y2r}+C_{y2l}\right)\cdot b}{m\cdot u_f}\cdot r+\\ &\frac{\left(C_{y1r}+C_{y1l}\right)}{m}\cdot\delta\end{aligned}$$

$$\begin{aligned}\dot{r} = &\frac{m\cdot h'\cdot\left(\dot{u}_f-r\cdot v\right)}{I_z}\cdot\varphi\\ &+\frac{\left(a\cdot\left(C_{y1l}-C_{y1r}\right)-b\cdot\left(C_{y2r}+C_{y2l}\right)\right)}{I_z\cdot u_f}\cdot v\\ &+\frac{\left(a^2\cdot\left(C_{y1l}-C_{y1r}\right)+b^2\cdot\left(C_{y2r}+C_{y2l}\right)\right)}{I_z\cdot u_f}\cdot r\\ &+\frac{a\cdot\left(C_{y1r}+C_{y1l}\right)}{I_z}\cdot\delta\end{aligned}$$

$$\dot{\varphi} = -\frac{\left(c_{\varphi 1} + c_{\varphi 2} - m \cdot g \cdot h'\right)}{k_{\varphi 1} + k_{\varphi 2}} \cdot \varphi - \frac{m \cdot h' \cdot u_f + \left(m \cdot h'^2 + I_y - I_z\right) \cdot r}{k_{\varphi 1} + k_{\varphi 2}} \cdot r$$

$$F_{x1r} = \frac{M_{fr1r} + M_{rb}/2}{R} - \frac{I_w \cdot \dot{u}_f}{R} \approx \frac{M_{fr1r} + M_{rb}/2}{R}$$

$$F_{x1l} = \frac{M_{fr1l} + M_{rb}/2}{R} - \frac{I_w \cdot \dot{u}_f}{R} \approx \frac{M_{fr1l} + M_{rb}/2}{R}$$

$$F_{x2r} = \frac{M_{fr2r}}{R} - \frac{I_w \cdot \dot{u}_f}{R} \approx \frac{M_{fr2r}}{R}$$

$$F_{x2l} = \frac{M_{fr2l}}{R} - \frac{I_w \cdot \dot{u}_f}{R} \approx \frac{M_{fr2l}}{R}$$